ADVANCED PHOTONICS RESEARCH Open Access
www.adpr-journal.com

Magnetron Sputter Deposition of Amorphous Silicon–SiO_2 Quantized Nanolaminates

Silvia Schwyn Thöny, Manuel Bärtschi, Marietta Batzer, Manuel Baselgia, Raphael Gmünder, Amit Sharma, Tijmen Vermeij, Xavier Maeder, and Stephan Waldner*

Quantization effects in nanolaminate structures of oxide materials are proposed and experimentally demonstrated only recently. Herein, the material combination of amorphous silicon and SiO_2 deposited by magnetron sputtering is investigated and it is shown that the quantization effect can be observed indeed. Transmission electron microscopy characterization gives evidence of continuous layers of amorphous silicon and SiO_2 with well-defined interfaces. The deposition process is described and the tunability of the refractive index and the bandgap energy is demonstrated. By doing so, the advantages of this novel material over classical optical materials are shown and feasibility is proved. As an example, a longpass optical interference filter with edge at 720 nm is deposited using quantized nanolaminates as the high and SiO_2 as the low refractive index material. This filter can be deposited successfully with close match to the design. It shows a blocking range throughout the visible spectrum whereas a comparable filter based on SiO_2–TiO_2 only blocks 500–700 nm.

1. Introduction

Optical interference coatings such as antireflection, mirror or filter coatings are based on stacks of materials with at least two different refractive indices, n. The interference effect is stronger if the difference in refractive index between materials is larger. Hence, a stack design based on materials with a larger difference in refractive index requires a smaller number of individual layers and thus less overall thickness to fulfill the same specification as a design based on materials with a smaller difference. In addition to the refractive index, the materials have to fulfill other requirements, among those being transparent with negligible losses in the wavelength range of interest.

However, in dielectric materials the refractive index and absorption edge are linked.[1] Materials with high refractive index have their absorption edge at a long wavelength, while low refractive index materials have the absorption edge at a short wavelength. TiO_2 is the dielectric material with the highest refractive index, which is transparent in the visible range (VIS) of the spectrum starting to transmit at ≈400 nm. Having a material at disposition with a higher refractive index while being transparent in the VIS would be of broad practical relevance because it would allow interference designs with a lower number of layers and reduced overall thickness. As will be shown in this article, the deposition rate of the nanolaminates exceeds the one of TiO_2. Both reduced thickness and high deposition rate are expected to result in increased productivity of the coating systems and reduced manufacturing cost.

Apart from the fabrication of nanolaminates, one approach to decouple the refractive index from bulk material properties is glancing angle deposition,[2,3] in which a columnar film structure is formed, which reduces the effective refractive index. Thus, interference effects will occur between bulk-like layers and layers with columnar structure of one and the same material. This opens up interesting effects such as plate polarizers or higher laser damage resistance due to the absence of interfaces between different materials.

A comparable approach are the self-organizing structures formed by ion etching of organic films as described by refs. [4,5]. Again, the effective refractive index of the layer is reduced by etching, which introduces localized and unlocalized porous structures.[6] This effect is beneficial, if the layer is used as the outermost layer in an antireflection design. As for glancing angle deposition, the drawback of the self-organizing layers is the increased sensitivity to environmental conditions.

A more recent concept to overcome the connection between the two characteristics is quantized nanolaminates (QNLs), which were first reported by Willemsen, Jupé et al. in 2016[7] and investigated in more detail in refs. [8,9]. In this concept, thin

S. S. Thöny, M. Batzer, M. Baselgia, R. Gmünder, S. Waldner
Evatec AG
Hauptstrasse 1a, 9477 Trübbach, Switzerland
E-mail: silvia.schwyn-thoeny@evatecnet.com

M. Bärtschi
RhySearch
Werdenbergstrasse 4, 9471 Buchs, Switzerland

A. Sharma, T. Vermeij, X. Maeder
Laboratory for Mechanics of Materials and Nanostructures
Empa, 3602 Thun, Switzerland

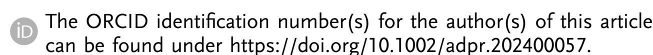
The ORCID identification number(s) for the author(s) of this article can be found under https://doi.org/10.1002/adpr.202400057.

© 2024 The Author(s). Advanced Photonics Research published by Wiley-VCH GmbH. This is an open access article under the terms of the Creative Commons Attribution License, which permits use, distribution and reproduction in any medium, provided the original work is properly cited.

DOI: 10.1002/adpr.202400057

26999293, 0, Downloaded from https://onlinelibrary.wiley.com/doi/10.1002/adpr.202400057 by Schweizerische Akademie Der, Wiley Online Library on [12/08/2024]. See the Terms and Conditions (https://onlinelibrary.wiley.com/terms-and-conditions) on Wiley Online Library for rules of use; OA articles are governed by the applicable Creative Commons License

layers of high and low refractive index with a thickness in the nanometer range or below are stacked. The limited structure size leads to a change of the energy gap, which can be adjusted by the physical thickness of the materials, whereas the thickness ratio of the materials determines the effective refractive index of the QNL. Similar effects are observed in multiquantum well structures of crystalline material. However, Willemsen et al.[10] have shown in their investigations that the crystalline structure is by no means the precondition for the occurrence of quantum effects, but that they can also be observed in amorphous dielectric materials.

In optical interference coatings, the decoupling of bandgap and refractive index potentially offers the advantage of using the QNL material combination instead of using a specific material. As an example, in the UV range the bandgap of Ta_2O_5 can be pushed toward shorter wavelength and can thus replace the use of HfO_2. This is desirable because hafnium targets are expensive and because HfO_2 has a tendency to form polycrystalline films with grain boundaries which can cause losses by straylight. First demonstrations of this approach are given in refs. [7–9].

The article by Henning et al.[11] explains that the combination of amorphous silicon (aSi) and SiO_2 has the potential to be transparent even in the visible wavelength range with an effective refractive index higher than 2.7. In a recent article,[12] Kreuzer et al. show results of magnetron sputtered aSi/SiO_2 nanolaminates using cylindrical targets with varying aSi layer thicknesses and compositions. A shift in bandgap is observed. However, Kreuzer et al. state that this shift is approximately one order of magnitude smaller than expected.

It is thus the scope of this article to investigate a wide parameter field for the deposition of nanolaminates of aSi–SiO_2 by magnetron sputtering from a planar target and to demonstrate the potential of optical interference coatings using the nanolaminate as high index material.

Nanolaminates showing the quantization effect were demonstrated experimentally for dielectrics such as SiO_2 combined with Ta_2O_5, HfO_2, or Al_2O_3, but not for aSi–SiO_2. The deposition methods reported are atomic layer deposition (ALD), ion beam sputtering (IBS),[7–9] and magnetron sputtering.[12,13] Although ALD and IBS lead to good results, they do have drawbacks with regard to volume production, whereas magnetron sputtering was demonstrated on a volume production machine with deposition rates comparable to standard values.

As reported in ref. [13], the turntable configuration of the Evatec CLUSTERLINE 200 BPM magnetron sputter system is ideally suited for the deposition of QNL because both materials, SiO_2 and Ta_2O_5, can be deposited in one table rotation. We will show in this article how the process for the material combination aSi and SiO_2 is implemented in this magnetron sputter deposition system. This time the sputter source is used for the deposition of aSi, whereas the SiO_2 is formed when passing a plasma source operated with oxygen that generates reactive atomic oxygen neutrals and ions. Again, the turntable exposes the growing film sequentially to both sources. A series of experiments was conducted, in which the thicknesses of individual layers in the nanolaminate was varied by changing the speed of the table rotation. With these experiments we will demonstrate that the quantum effect is observed as predicted in ref. [12]. Furthermore, the structure of the aSi/SiO_2 QNL is analyzed by transmission electron microscopy (TEM). We will then take these results and show that a longpass filter blocking the vis and transmitting from 700 nm onward can be realized with just 16 layers combining SiO_2 and QNL based on aSi–SiO_2.

2. Theory

As mentioned in the introduction, in standard dielectric materials the refractive index and the energy of the absorption gap are fundamentally linked.[1] Quantized nanolaminates proposed in refs. [7–9], however, allow to set the refractive index and the absorption edge independently within the limits given by the bulk properties of the high and low index material.

The theory of the quantized nanolaminates is detailed in the publications[7–9] and summarized hereafter for the sake of clarity. First of all, a brief look at the electronic material properties is necessary. As already mentioned, optical coatings mostly produce amorphous or polycrystalline materials whose band structure is not clearly defined; nevertheless, an energy gap between quasi-free ground states and higher conduction states is present. Thus, the bandgap itself can be regarded as a depletion zone of states and the densities between bound and free states are so low that they can be neglected. Thus, the potential well, which is necessary for the quantization, is clearly defined.

The electron mobility can be limited in the growth direction if two materials with high and low bandgap are combined in a thin periodic structure. In this case, the low index material will act as a barrier, whereas the high index material acts as the quantum well, as illustrated in **Figure 1**. As this is a simple potential consideration, even nonclosed atomic layers can lead to a suitable periodic potential.

The thickness of the quantum well will determine the shift in bandgap, whereas the thickness ratio of high-to-low bandgap material will determine the refractive index. Thus, the novel concept of so-called QNLs allows for independent adjustment of the optical bandgap and the refractive index. To give an idea of the thicknesses required, we turn to data published for SiO_2–Ta_2O_5 in ref. [13], which shows that the quantum well layer should be much smaller than 2 nm to achieve a shift, which is of practical use.

3. Experimental Section

The quantized nanolaminates were deposited using a Clusterline 200 BPM magnetron sputter deposition system manufactured

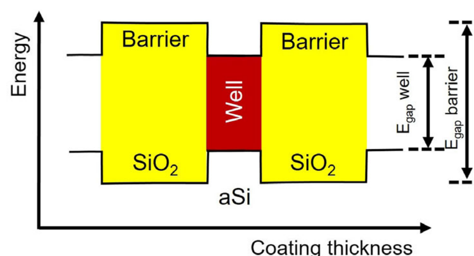

Figure 1. Periodic structure of high and low bandgap areas, which limit the electron mobility.

© 2024 The Author(s). Advanced Photonics Research published by Wiley-VCH GmbH

26999293, 0, Downloaded from https://onlinelibrary.wiley.com/doi/10.1002/adpr.202400057 by Schweizerische Akademie Der, Wiley Online Library on [12/08/2024]. See the Terms and Conditions (https://onlinelibrary.wiley.com/terms-and-conditions) on Wiley Online Library for rules of use; OA articles are governed by the applicable Creative Commons License

by Evatec, which was discussed in detail in refs. [14–16]. For the sake of clarity, we will summarize the main parts of the system as well as the mode of operation in this Experimental Section. As shown in **Figure 2**a, the system uses a sputter down configuration with a maximum of four magnetron sputter sources denoted with (1). For the deposition of aSi–SiO_2 QNL, one sputter source was equipped with a silicon target with the purpose to deposit an aSi layer. The SiO_2 layer is formed by the plasma source (PSC) (2), where the aSi film partially gets oxidized by the oxygen plasma. The plasma source is a RF-driven capacitively coupled discharge, where oxygen as operating gas is partially dissociated and ionized. The schematic tool configuration is shown in Figure 2b.

When depositing the longpass filter consisting of aSi–SiO_2 QNL as the high refractive index material and SiO_2 for the low refractive index material, a second sputter station equipped with a silicon target was used to reactively deposit the low index SiO_2 layers.

The turntable configuration is perfectly suited for the deposition of QNL. With the continuous table rotation substrates pass repeatedly beneath the active sources, thereby exposing the substrates to both the sputter and the plasma source with each rotation. The total thickness deposited in one turn is determined by the rotation speed of the table, a parameter which can easily be varied in a wide range, and the deposition rate. The thickness ratio of the aSi and SiO_2 materials is determined by the sputter and the plasma source power, which can be adjusted individually. Further deposition parameters, which influence the deposition rate and material properties are the gas flows of argon and oxygen. Deposition rates for QNL layers tend to be as high as those for single aSi because the active source is run at standard conditions.

This deposition system has a capacity of 15 substrates of diameter 200 mm. Substrate loading and unloading is executed automatically through a vacuum transfer module and load-lock. The system is also equipped with broad band and monochromatic optical monitoring.[17]

The samples were deposited on double side polished fused silica substrates. These were characterized by spectrophotometry in transmission T and reflection R both at an angle of 8° on the exact same spot on the sample by using a PhotonRT photospectrometer by EssentOptics.

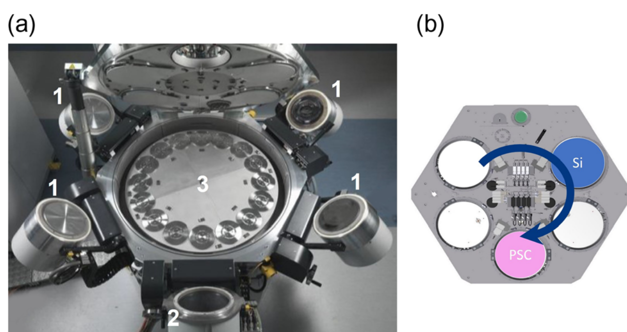

Figure 2. a) Evatec Clusterline BPM magnetron sputter system opened to maintenance position: sputter sources (1), plasma source (2), and turn table (3). b) Schematic of sputter process for the QNL layers of aSi–SiO_2.

The effective refractive index n_{eff} and the extinction coefficient k in the transparent range of the coating were determined using OptiChar by Optilayer. The models used were normal dispersion for n and UV–vis mode for the extinction coefficient k. This evaluation also allows us to determine the physical thickness d of the nanolaminate stack.

The same commonly high accuracy methodology is used to determine the properties of the standard dielectrics, in our case SiO_2 and aSi. Their optical constants serve as a reliable input for a rather simple, but robust evaluation procedure based on the concept of Wiener bounds limit.[18,19] In mixed component systems, the refractive index can be modeled by applying the effective medium theory.[20] The effective refractive index of the resulting metamaterial n_{eff} is determined by the volumetric fraction f of the high refracting material in the QNL

$$n_{eff}^2(\lambda) = f\, n_{high}^2(\lambda) + (1-f)\, n_{low}^2(\lambda) \tag{1}$$

The effective refractive index n_{eff} is derived from the spectral measurements in T and R as detailed above. The refractive indices of n_{high} and n_{low} are determined from aSi and SiO_2 single layers. The values used were: aSi $n_{high} = 3.937$ and SiO_2 $n_{low} = 1.466$, both indices relate to a wavelength of 1000 nm. Equation (1) then allows us to calculate the volume fraction f of the two materials. This simple formula shows that the refractive index of the QNL is always between the values of the high and low refractive index materials and defines the physical refractive index limits of the nanolaminate.

The thickness per table pass can be calculated by dividing the physical thickness d of the nanolaminate stack by the number of passes in the deposition. The thickness of the individual high and low refractive index layers in the QNL can then be calculated by multiplying the total thickness per pass with the volume fraction f of the high index material, respectively (1-f) for the low index material.

The Tauc-plot method[21] was used to determine the optical bandgap based on the optical absorption coefficient calculated from the spectrophotometric measurements in transmission and reflection.

All samples used in this article underwent an annealing step at 500 °C for 1 h in air. These conditions led to the lowest loss values, based on the results of a series of annealing tests involving variations in time and temperature.

The structure of the aSi–SiO_2 QNL was characterized by scanning transmission electron microscopy (STEM) imaging using a Themis 200 G3 spherical aberration (probe)-corrected TEM (Thermo Fischer, Waltham, USA), operated at 200 kV. This was performed on thin lamellae of the cross section of the coating, prepared via focused ion-milling (FIB lift-out technique) using a dual beam FIB-SEM Tescan Lyra FEG system (Brno, the Czech Republic). The FIB parameters for the lift-out were 30 kV and 3 nA for the rough cutting and 30 kV and 500 pA for the polishing. The lamella was thinned down to 30 nm using 30 kV with 100 and 50 pA, with a final polishing at 5 kV with 50 pA. Elemental distribution and concentration line profile were acquired using energy-dispersive spectroscopy in STEM mode.

© 2024 The Author(s). Advanced Photonics Research published by Wiley-VCH GmbH

26999293, 0, Downloaded from https://onlinelibrary.wiley.com/doi/10.1002/adpr.202400057 by Schweizerische Akademie Der, Wiley Online Library on [12/08/2024]. See the Terms and Conditions (https://onlinelibrary.wiley.com/terms-and-conditions) on Wiley Online Library for rules of use; OA articles are governed by the applicable Creative Commons License

4. Results

4.1. Quantum Nanolaminate Layers of aSi–SiO_2

In a first experiment, the Si sputter source and plasma source were run at 5 and 1 kW, respectively. When the sample passes the sputter source, a film of aSi is deposited. With the table rotation this sample is then translated to pass beneath the plasma source where a part of the previously deposited aSi layer gets oxidized. This sequence is repeated for a defined coating time.

In a first experiment, the table speed was varied from 1.5 to 12 s per pass, resulting in an increasing thickness of the individual nanolaminate layers. The coating time was fixed for this series of four samples and resulted in a nanolaminate stack thickness of ≈180 nm. The number of individual nanolaminate layers varies from 300 to 38 corresponding to 1.5–12 s/pass. In **Figure 3**, the curves of the spectrophotometric measurements in transmission of the 4 runs reveal three characteristics of the layers: first, the wavelength of the absorption edge, second, the losses in the transparent wavelength range, and third, the refractive index of the layers.

First, the absorption edge of this series of deposition runs shifts toward shorter wavelength the faster the table speed. The absorption edge of the sample with 1.5 s/pass lies at the shortest wavelength, whereas 12 s/pass results in the longest wavelength with a difference of ≈280 nm between the samples at a fixed transmission of 75%. For comparison, the black dashed line indicates the onset of transmission of a regular aSi layer.

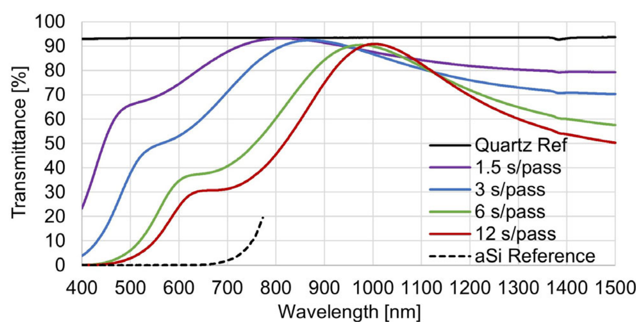

Figure 3. Transmittance spectra of QNL layers with the same power ratio of aSi to PSC, but with table speeds (1.5/3/6/12 s/pass).

Second, the transmission maxima at $\lambda/2$ optical thickness closely touch the solid line of the uncoated quartz indicating low absorption of the QNLs in the longer wavelength range.

Third, the transmission at 1500 nm increases with table speed. This is indicative of a reduction in effective refractive index of the nanolaminates. In the following we will first explain the shift in refractive index and then the shift in the absorption edge.

As explained in the Experimental Section, the effective refractive index n_{eff} and the total layer thickness d_{tot} can be determined from the transmission and reflection measurements in the transparent region. The thickness deposited per table turn can then be obtained by dividing d_{tot} by the number of table-turns. As expected, the thickness deposited per turn is linear with the table speed, as can be seen in **Figure 4**a. However, the individual thicknesses of aSi to SiO_2, calculated according to Equation (1), do not increase linearly as can be seen from Figure 4b. In the run with the fastest table speed, an aSi layer of 0.7 nm thickness was deposited, which was subsequently oxidized by the oxygen plasma of the PSC to an SiO_2 layer with a thickness of 0.6 nm. For the slowest table speed of 12 s/pass however, the 4.2 nm aSi only gets oxidized to a thickness 1.8 nm SiO_2. The decrease in oxidized thickness is expected: the energetic oxygen species generated in the plasma source have a limited penetration depth even if the exposure time is extended. In consequence, thicker layers have a reduced fraction of SiO_2, which, in turn, will lead to a higher refractive index of the nanolaminate as can also be seen in Figure 4b on the right axis.

In a next step, we will take a look at the shift of the absorption edge. The strong shift in absorption edge, as shown in Figure 3, can mainly be attributed to the change of the average stoichiometry over the total thickness of the nanolaminate stack as explained above. In order to see whether a quantum effect is present, films with increasing individual nanolaminate thicknesses, but constant thickness ratio of aSi and SiO_2 have to be compared. For this to be the case, adjustments had to be made in the process settings such as Si source power and oxygen flow.

An example of such an experiment is shown in **Figure 5**a: runs 1–3 have a very close thickness ratio of aSi:SiO_2 of around 0.68, as can be seen from the overlaying minimum transmission value at 1650 nm. Thus, these films have the same refractive index and average composition, but decreasing total thickness per pass of 2.3, 1.1, and 0.5 nm. The transmission measurement of the three runs shows a shift in absorption edge of 57 nm. We will clarify now whether these films are mixtures, and the edge shift is due

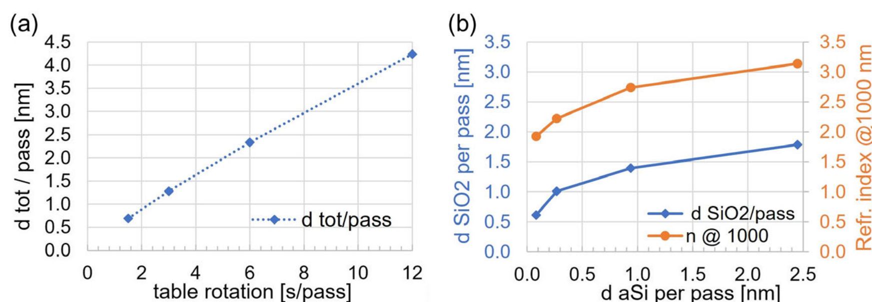

Figure 4. a) The total thickness per pass increases linearly with increasing time per pass. b) Lower increase of the SiO_2 thickness compared to aSi (left axis) which leads to an increase in refractive index (right axis).

© 2024 The Author(s). Advanced Photonics Research published by Wiley-VCH GmbH

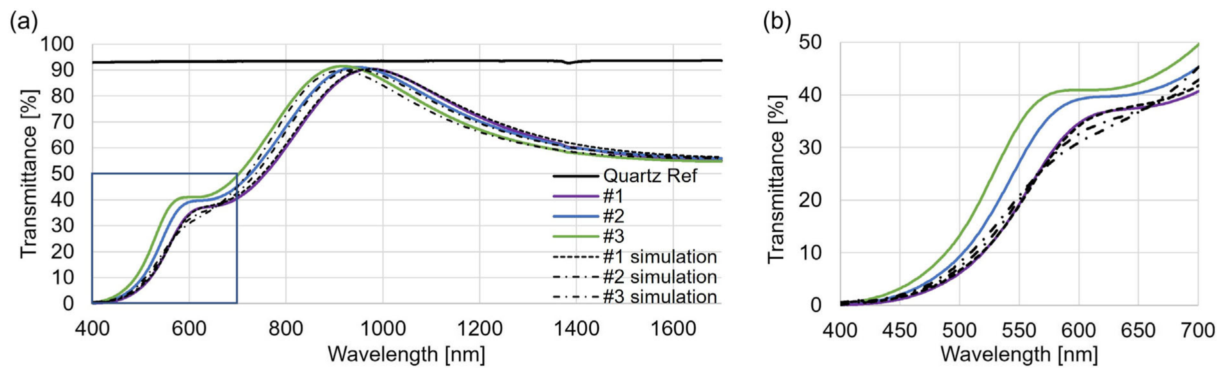

Figure 5. a) Shift of absorption edge in transmission of three films with the same thickness ratio of aSi:SiO_2 but decreasing individual nanolaminate thickness. b) Inset of the absorption region showing the simulation of the mixture in dashed lines.

to the slightly different stack thickness or whether the shift is due to the quantization effect. To evaluate the first hypothesis the dispersion of the refractive index and extinction coefficient for run 1 is determined. In accordance with the assumption of a mixture, the transmission curves for the 3 thicknesses are simulated, based on the same dispersion values. The three curves shown as dashed lines in Figure 5 overlay at the absorption edge; thus, the effect cannot be explained with mixture materials. Hence, the edge shift of these layers with different nanolaminate thickness, but constant material ratio can be attributed to the quantization effect as explained in the theory section.

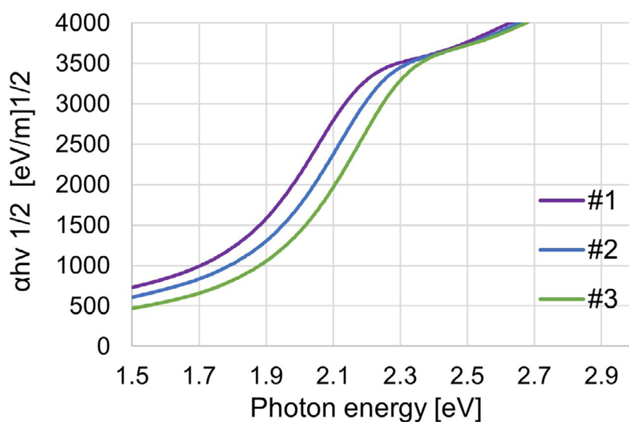

Figure 6. Tauc plot of samples 1–3 showing the shift in bandgap energy.

The final confirmation of quantization is seen in the shift of the bandgap energy in **Figure 6**, which was determined from the Tauc plot as described in ref. [21]. The gap energy increases with the decreasing aSi well thickness of samples 1–3 by 0.14 eV, which corresponds to a shift of 58 nm in wavelength. This result determined on three different nanolaminates with the same composition and refractive index confirms that the quantization effect can be observed in the material system aSi–SiO_2 deposited by magnetron sputtering.

As mentioned in the Experimental Section, all samples shown so far were annealed at 500 °C in air ambient. **Figure 7**a shows the losses (100%–T–R) of samples 1–3 before and after annealing. Two effects can be observed: a faster decay of losses in the transmission region and a shift of the absorption edge toward shorter wavelength for samples with annealing. The relative edge shift between samples is very similar in pre- and postannealed samples as can be seen in Figure 7b, confirming that the nanolaminate structure and quantization effect are preserved upon annealing. It is worth noting, that for the present samples an increased shift of the gap energy is observed the thinner the barrier. However, for even thinner barriers tunneling is expected to set in and hence the gap shift will reduce.

Figure 7b shows that the refractive index among the samples is in a very narrow band but shows a reduction of ≈0.04 after annealing. This indicates that the annealing effect is independent of the thickness of individual aSi and SiO_2 layers. The refractive index after annealing remains high at $n \approx 2.75$ ($\lambda = 1000$ nm), which implicates that if oxidation is the origin of the reduction

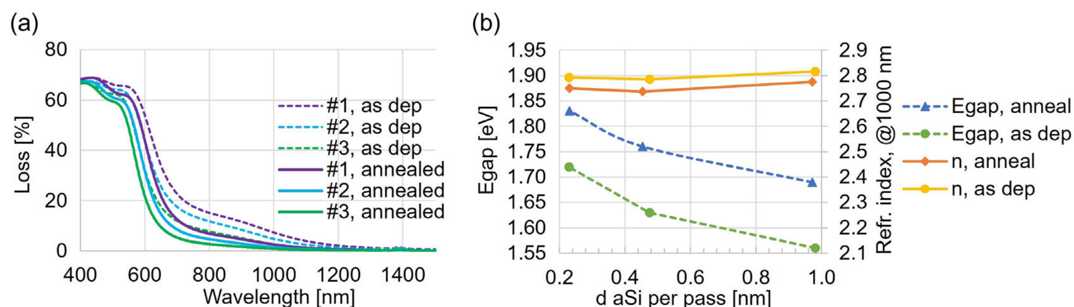

Figure 7. a) Losses decrease for the samples after annealing. b) Refractive index and gap energy for samples before and after annealing.

© 2024 The Author(s). Advanced Photonics Research published by Wiley-VCH GmbH

26999293, 0, Downloaded from https://onlinelibrary.wiley.com/doi/10.1002/adpr.202400057 by Schweizerische Akademie Der, Wiley Online Library on [12/08/2024]. See the Terms and Conditions (https://onlinelibrary.wiley.com/terms-and-conditions) on Wiley Online Library for rules of use; OA articles are governed by the applicable Creative Commons License

of the index, the effect is small (a few percent in thickness) and precludes a substantial oxidation of aSi layers to SiO_2. To clarify the nature of the changes, dedicated TEM analysis will be conducted to get insight into the effect of annealing.

Subsequently, experiments were performed varying different deposition parameters. **Figure 8** shows the dependence of the gap energy and the refractive index with oxygen flow in the plasma source for a series of runs with table speed of 1.5 s/pass. With an increasing availability of oxygen in the plasma, the SiO_2 nanolayer thickness increases and thus the refractive index decreases while the gap energy, in turn, increases. The full evaluation as well as additional experiments to push the QNL effect further will be the scope of future work.

4.2. TEM Characterization

A STEM high-angle annular dark-field (HAADF) image of the entire cross section of an aSi–SiO_2 QNL deposited on fused silica is shown in **Figure 9**, with an increase of the magnification in the figure inset. This is the sample shown in Figure 3 deposited with 6 s/pass. The coating has a total thickness of 179.5 nm with 75 bilayers. The layering contrast is coming from the slight difference in density between the aSi and SiO_2 layers, the bright layers being the SiO_2. The STEM images show that the layers are continuous with a sharp and very well-defined interface between the aSi and the SiO_2 layers. The mean thickness of the aSi and SiO_2 layers is 0.95 and 1.52 nm, respectively. These values are in good agreement with the thicknesses calculated from the optical measurements being 0.9 and 1.45 nm with a total thickness of 175.5 nm. An additional periodicity in layer thickness is seen in the STEM images and is in the focus of further investigations.

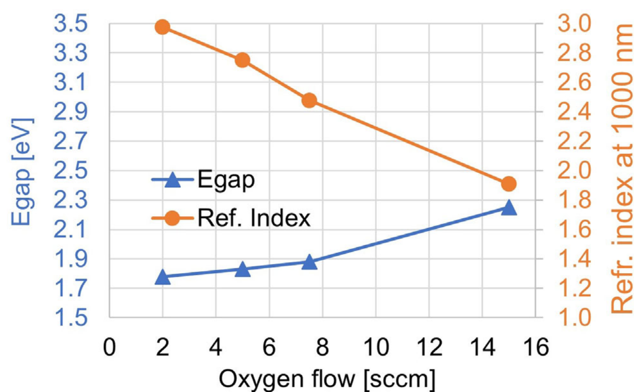

Figure 8. An increase of the oxygen flow in the PSC leads to a decrease in refractive index and an increase in E_{gap}.

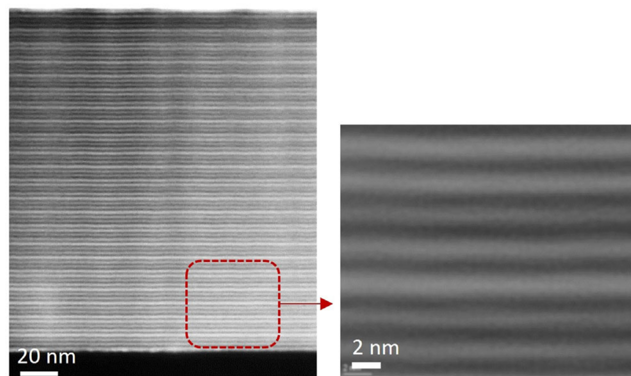

Figure 9. STEM HAADF image of the entire cross section of an aSi–SiO_2 QNL. The figure inset shows the details of the nanolaminates.

4.3. Longpass Filter

As shown in the previous section, QNL can be manufactured with a wide range of refractive indices and gap energies. The nanolaminate of run #3 from Section 4.1 was chosen as the high and SiO_2 as low refractive index material to deposit a longpass filter. As described in the Experimental Section, the QNL was deposited using the aSi sputter source in combination with the plasma source, whereas the SiO_2 layers were deposited from the additional sputter source. A design was chosen with 16 layers of $\lambda/4$ optical thickness with some of the outer layers being adjusted to provide an edge formed curve. Material #3 has a refractive index of 3.18 and 2.75 at wavelength 550 and 1000 nm, respectively, and E_{gap} of 1.83 eV. In this case, a high index layer with optical thickness of $\lambda/4$ at 600 nm has a physical thickness of 49 nm and consists of a total of 180 alternating layers of aSi and SiO_2. Thanks to the turn table configuration of the BPM magnetron sputter deposition system, the deposition rate of the nanolaminate is as high as for a standard aSi layer.

Figure 10 shows the measured spectrum of the longpass filter. It confirms that this filter indeed blocks the entire visible part of the spectrum and transmits the near-infrared (NIR) part. For reference, the analogous design using standard aSi as high index material will suffer from high losses in the wavelength region of 700–900 nm and only reach full transparency beyond 1000 nm; this is due to the absorption edge at higher wavelength.

In situ broadband optical monitoring in reflection in a wavelength range of 380–980 nm was used to monitor the coating thickness. It turned out that the reflection signal of the QNL developed completely regular, exactly as a layer with the corresponding effective refractive index would evolve. We can therefore conclude that optical monitoring is perfectly suited for controlling the thickness in film stacks with QNLs.

For comparison, the same type of filter was coated based on the standard material combination SiO_2–TiO_2 also using 16

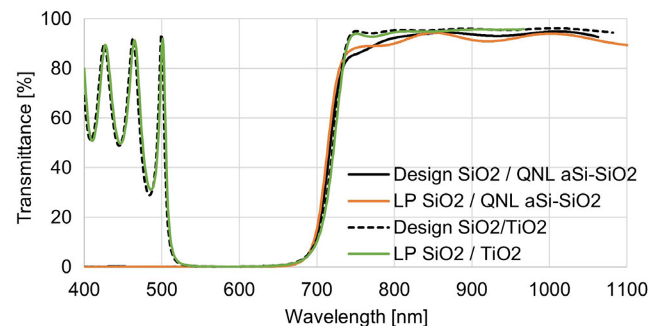

Figure 10. Transmittance of a longpass filter based on SiO_2/QNL aSi–SiO_2 and on SiO_2–TiO_2 for comparison.

© 2024 The Author(s). Advanced Photonics Research published by Wiley-VCH GmbH

26999293, 0, Downloaded from https://onlinelibrary.wiley.com/doi/10.1002/adpr.202400057 by Schweizerische Akademie Der, Wiley Online Library on [12/08/2024]. See the Terms and Conditions (https://onlinelibrary.wiley.com/terms-and-conditions) on Wiley Online Library for rules of use; OA articles are governed by the applicable Creative Commons License

layers, based on the same design principle as the nanolaminate filter. In Figure 10, it becomes immediately apparent that the standard design does only block half of the visible range, whereas the QNL design blocks the entire range. Of course, it is possible to reach full blocking with an SiO_2–TiO_2 design, however at the expense of double the number of layers.

The standard coating has a total thickness of 1.4 μm as compared to 1 μm for the QNL–SiO_2 design. Furthermore, the deposition rate of the QNL is about double the rate of TiO_2. Both reduced thickness and increased deposition rate result in a cut of the deposition time by a factor of 2. Thus, this comparison shows the large potential of the new nanolaminate material to significantly boost productivity and reduce manufacturing cost.

5. Conclusion

As demonstrated in this article, magnetron sputtering using a deposition tool with turntable configuration is ideally suited to depositing quantum nanolaminate layers. The individual layers of the nanolaminate stack are deposited sequentially, the aSi when passing under the silicon source and the SiO_2 by oxidation of the top part of the aSi layer when passing the plasma source. This sequence is repeated with every rotation of the turntable. The setting of the table rotation speed allows to select the total thickness of aSi and SiO_2 per turn, whereas the power setting of the sputter and plasma sources allows to set the thickness ratio of aSi and SiO_2. We demonstrated individual layers with a few tenth of nm and a wide range of aSi volumetric fractions f of 0.1–0.75.

The single layers show a large shift in the absorption edge. The analysis of the data revealed two mechanisms causing the shift. As a first effect, a change in composition leads to a shift of the absorption edge to shorter wavelength the higher the SiO_2 fraction in the film. This is an effect, which is well known. The second effect, however, caused by quantization, is demonstrated using aSi–SiO_2 QNL with the same average composition: they show a shift in absorption edge when the thickness of the aSi barrier layer decreases while the refractive index is constant. This is in accordance with theory, as described in Section 2.

The TEM analysis confirms that continuous layers with sharp and well-defined interfaces are present in the QNL.

In a next step, QNL layers were used as the high index material in an optical interference filter. We demonstrated that the turntable configuration of the sputter system leads to a viable manufacturing process for this longpass filter blocking the visible part of the spectrum while transmitting the NIR. From a technical standpoint, the deposition of these filters runs like a standard process with the difference that in the QNL layer two sources are powered. Furthermore, optical monitoring can also be used without any adaption.

The longpass filter coating was in good agreement with the design and showed good transmission in the wavelength range above 700 nm, thus confirming the precise and reproducible deposition in the sub-nm range. As a comparison, a standard SiO_2/TiO_2 longpass filter was also deposited. This showed that with the same number of layers the blocking range was much narrower than for the QNL design. For a standard filter with the same characteristic as the QNL filter, double the number of layers would be required. This clearly shows that the concept of QNL indeed opens up a wide field for novel applications with significant improvements in productivity.

Acknowledgements

The authors thank Innosuisse—Swiss Innovation Agency for funding Project 110.023 IP-ENG.

Conflict of Interest

The authors declare no conflict of interest.

Data Availability Statement

The data that support the findings of this study are available from the corresponding author upon reasonable request.

Keywords

bandgap, low-loss coating, magnetron sputtering, meta materials, optical thin films, quantized nanolaminates

Received: April 4, 2024
Revised: June 13, 2024
Published online:

[1] H. Finkenrath, *Infrared Phys.* **1988**, *28*, 327.
[2] T. Tolenis, L. Grineviciute, L. Smalakys, M. Ščiuka, R. Drazdys, L. Mažule, R. Buzelis, A. Melninkaitis, *Sci. Rep.* **2017**, *7*, 10898.
[3] L. Grineviciute, M. Andrulevicus, A. Melninkaitis, R. Buzelis, A. Selskis, A. Lazauskas, T. Tolenis, *Phys. Status Solidi A* **2017**, *214*, 1700764.
[4] U. Schulz, *Appl. Opt.* **2006**, *45*, 1608.
[5] U. Schulz, F. Rickelt, P. Munzert, N. Kaiser, *Opt. Mater. Express* **2014**, *4*, 568.
[6] H. Badorreck, M. Steinecke, L. Jensen, D. Ristau, M. Jupé, J. Müller, R. Tonneau, P. Moskovkin, S. Lucas, A. Pflug, L. Grinevičiūtė, A. Selskis, T. Tolenis, *Opt. Express* **2019**, *27*, 22209.
[7] T. Willemsen, P. Geerke, M. Jupe, L. Gallais, D. Ristau, *Proc. SPIE* **2016**, *10014*, 100140C.
[8] M. Jupé, T. Willemsen, H. Liu, M. Steinecke, L. Jensen, D. Ristau, in *Optical Interference Coatings Conf.*, Santa Ana Pueblo, New Mexico, USA **2019**.
[9] M. Steinecke, H. Badorreck, M. Jupé, T. Willemsen, L. Hao, L. Jensen, D. Ristau, *Appl. Opt.* **2020**, *59*, A236.
[10] T. Willemsen, M. Jupé, M. Gyamfi, S. Schlichting, D. Ristau, *Opt. Express* **2017**, *25*, 31948.
[11] P. Henning, M. Jupé, S. Bruns, T. Melzig, M. Steinecke, A. Wienke, M. Vergoehl, in *Optical Interference Coatings*, **2019**.
[12] K. Kreuzer, P. Henning, M. Vergoehl, S. Bruns, T. Melzig, C. Patzig, R. Feder, *Appl. Opt.* **2024**, *63*, 1641.
[13] S. S. Thöny, M. Bärtschi, M. Batzer, M. Baselgia, S. Waldner, M. Steinecke, H. Badorreck, A. Wienke, M. Jupé, *Opt. Express* **2023**, *31*, 15825.
[14] S. S. Thöny, M. Chesaux, S. Gees, A. Frigg, in *Optical Interference Coatings Conf.*, Tucson, Arizona, USA **2016**.

© 2024 The Author(s). Advanced Photonics Research published by Wiley-VCH GmbH

26999293, 0, Downloaded from https://onlinelibrary.wiley.com/doi/10.1002/adpr.202400057 by Schweizerische Akademie Der, Wiley Online Library on [12/08/2024]. See the Terms and Conditions (https://onlinelibrary.wiley.com/terms-and-conditions) on Wiley Online Library for rules of use; OA articles are governed by the applicable Creative Commons License

[15] M. Chesaux, S. S. Thöny, S. Gees, A. Frigg, in *Optical Interference Coatings Conf.*, Tucson, Arizona, USA **2016**.
[16] S. S. Thöny, S. Gees, E. Schüngel, in *Optical Interference Coatings Conf.*, Santa Ana Pueblo, New Mexico, USA **2019**.
[17] S. Waldner, J. Buchholz, R. Benz, in *Optical Interference Coatings Conf.*, Santa Ana Pueblo, New Mexico, USA **2019**.
[18] C. Franke, O. Stenzel, S. Wilbrandt, J. Wolf, N. Kaiser, A. Tünnermann, *Appl. Opt.* **2015**, *54*, 2362.
[19] R. Jansson, H. Arwin, *Opt. Commun.* **1994**, *106*, 133.
[20] A. Feldman, *Model. Opt. Thin Films* **1988**, *821*, 129.
[21] B. D. Viezbicke, S. Patel, B. E. Davis, D. P. Birnie, *Phys. Status Solidi B* **2015**, *252*, 1700.

© 2024 The Author(s). Advanced Photonics Research published by Wiley-VCH GmbH

26999293, 0, Downloaded from https://onlinelibrary.wiley.com/doi/10.1002/adpr.202400057 by Schweizerische Akademie Der, Wiley Online Library on [12/08/2024]. See the Terms and Conditions (https://onlinelibrary.wiley.com/terms-and-conditions) on Wiley Online Library for rules of use; OA articles are governed by the applicable Creative Commons License